Applied Surface Science 257 (2010) 817–822

Contents lists available at ScienceDirect

Applied Surface Science

journal homepage: www.elsevier.com/locate/apsusc

The optoelectronic properties of silicon films deposited by inductively coupled plasma CVD

Yanli Qin, Hengqing Yan, Fei Li, Li Qiao, Qiming Liu, Deyan He*

Department of Physics, Lanzhou University, Lanzhou 730000, China

ARTICLE INFO

Article history:
Received 7 May 2010
Received in revised form 12 July 2010
Accepted 20 July 2010
Available online 13 August 2010

Keywords:
Silicon films
Substrate temperature
Inductively coupled plasma
Optoelectronic properties

ABSTRACT

Hydrogenated amorphous and microcrystalline silicon films were deposited by inductively coupled plasma chemical vapor deposition (ICP-CVD) at low substrate temperatures using H_2-diluted SiH_4 as a source gas. High-density plasma generated by inductively coupled excitation facilitates the crystallization of silicon films at low temperatures, and microcrystalline silicon films were obtained at the substrate temperature as low as 180 °C. The columnar structure of the films becomes more and more compact with an increase of their crystallinity. The reduction of hydrogen content in the films causes a narrowing of the optical bandgap and an enhancement of the absorption with increasing the substrate temperature. The microcrystalline silicon films show two electronic transport mechanisms: one is related to the density of state distribution in the temperature region near room temperature and the other is the variable range hopping between localized electronic states close to the Fermi level below 170 K. A reasonable explanation is presented for the dependence of the optoelectronic properties on the microstructure of the silicon films. The films prepared at a substrate temperature of 300 °C have highly crystalline and compact columnar structure, high optical absorption coefficient and electrical conductivity, and a low hydrogen content of 3.8%.

© 2010 Elsevier B.V. All rights reserved.

www.spm.com.cn

1. Introduction

Silicon-based thin film solar cells have attracted more and more attention and been as a subject to extensively investigate aiming at improving the efficiency and cutting the cost. However, the photovoltaic conversion efficiency of a single junction solar cell is limited by the pass band of the active layer which does not cover the entire solar spectrum. An improved way is to build a multiple structure which is composed of several stacked layers with complementary values of the bandgap, so that the sunlight can be effectively absorbed over the solar spectrum [1,2]. To deposit microcrystalline silicon films with a tunable optical bandgap and an improved carrier transport for using in the tandem solar cells, some high-density plasma sources such as very high frequency plasma, inductively coupled plasma (ICP), microwave plasma and surface wave plasma [3–9] have been developed besides conventional capacitively coupled plasma. Among these technologies, ICP has been increasingly attracting more attention due to its unique characteristics of high electron density, low electron temperature, low plasma potential and the simplicity of the configuration [10,11]. The advantages of ICP provide an effective method to prepare the microcrystalline silicon films with excellent optoelectronic properties. Especially, large numbers of efforts have been done and many improvements have been made on the non-uniformity of ICP for mass deposition of large-area uniform films [12–16].

In this paper, hydrogenated amorphous and microcrystalline silicon films were deposited at low substrate temperatures by ICP-CVD using a mixture of H_2 and SiH_4. The effects of substrate temperature on the microstructure and optoelectronic properties of the silicon films were reported in detail.

2. Experimental

Hydrogenated amorphous and microcrystalline silicon films were deposited on p type c-Si (1 1 1) wafer and glass plate by ICP-CVD. The reactor is a stainless-steel cylinder with a diameter of 45 cm and a height of 50 cm. The plasma was generated by a built-in one-turn inductance coil (10 cm in diameter) made of a copper tube. In order to produce high-density and homogeneous plasma, the surface of the inductance coil was coated with a layer of 0.1-cm-thick fiberglass. In this work, the rather uniform amorphous and microcrystalline silicon films were deposited by varying the substrate temperature from 140 °C to 300 °C. The base vacuum was 1×10^{-3} Pa. During the deposition, radio frequency power, flow ratio of $[SiH_4]/([SiH_4] + [H_2])$ and total working gas pressure were kept at 300 W, 12% and 10 Pa, respectively.

* Corresponding author. Tel.: +86 931 8912546; fax: +86 931 8913554.
E-mail address: hedy@lzu.edu.cn (D. He).

0169-4332/$ – see front matter © 2010 Elsevier B.V. All rights reserved.
doi:10.1016/j.apsusc.2010.07.071

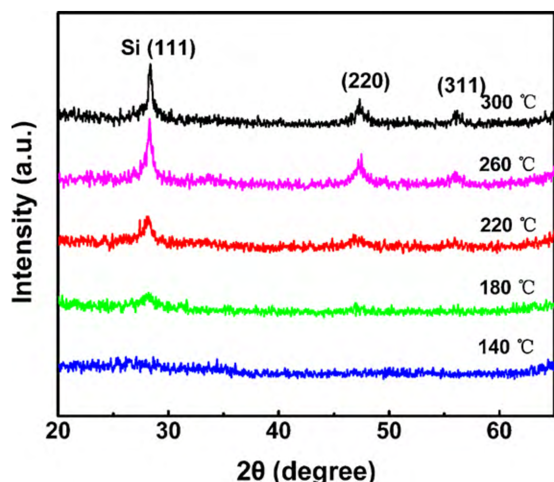

Fig. 1. XRD patterns of the silicon films deposited at various substrate temperatures.

The thickness of all the deposited films was between 700 and 800 nm.

The structure and morphology of the samples were characterized with X-ray diffraction (XRD), Raman spectroscopy, Fourier transform IR (FTIR), and atom force microscopy (AFM). XRD measurements were taken using a Rigaku D/Max-IIIC X-ray diffractometer with a Cu Kα source. Raman measurements were conducted by a Jobin-Yvon HR 800 spectrometer with an excitation wavelength of 532 nm. The IR absorption spectra were recorded using a FTIR spectrometer of Brucker IFS 66v/s in a range from 400 to 4000 cm^{-1}. The surface morphologies of the films were observed on a CSPM4000 AFM. To obtain the films' thickness and optical parameter, the optical transmission spectra were measured over a wavelength range of 400–2500 nm using a Shimadzu UV-3600 spectrometer at room temperature. The temperature-dependent dark conductivity was measured using a Keithley 6517A electrometer from 360 K down to 60 K at a constant rate of 1.5 K/min, and the activation energy was deduced based on an Arrhenius plot. Al coplanar electrodes were evaporated on the silicon films.

3. Results and discussion

3.1. Structure and morphology characterization

Fig. 1 shows the XRD patterns of the silicon films deposited at different substrate temperatures. The peaks at 28.6°, 47.3° and 56.1° for the films deposited at higher substrate temperatures are corresponding to Si (1 1 1), (2 2 0) and (3 1 1) crystal planes, respectively. No resolved peaks can be observed for the films deposited at a substrate temperature of 140 °C, indicating that the structure of the sample is amorphous. The appearance of the diffraction peaks with increasing the substrate temperature suggests the formation of silicon crystallites in the films. The grain size estimated from the width of (1 1 1) peak using Debye–Scherrer formula was summarized in Table 1. It can be seen that the film deposited at 300 °C has the maximum grain size, and the intensity of the (1 1 1) peaks for all the crystallized films is much higher than that of others, showing the films have a preferential growth along the (1 1 1) direction.

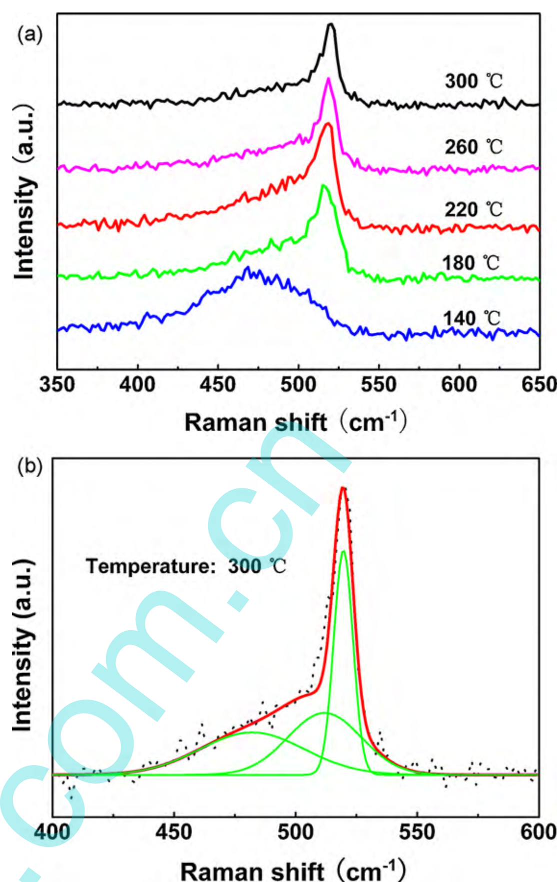

Fig. 2. (a) Raman spectra for the silicon films deposited at different substrate temperatures. (b) Deconvolution of the Raman spectra for the silicon films deposited at a substrate temperature of 300 °C.

The Raman spectra of the samples deposited at different substrate temperatures are shown in Fig. 2(a). The film deposited at 140 °C shows one broad band centered at 480 cm^{-1}, which means that the structure of the film is amorphous. When the substrate temperature increases to 180 °C, a dominant peak around 516 cm^{-1} emerges, implying the formation of small crystallites in the films. However, with a further increase of the substrate temperature, no obvious change can be observed in the Raman spectra. The bands in Raman spectra can be decoupled into three independent Gaussian peaks: a broad distribution centered at about 480 cm^{-1}, a sharp peak at 520 cm^{-1}, and an intermediate one around 510 cm^{-1} attributed to small crystallites or grain boundaries, as shown in Fig. 2(b) [17,18]. The crystalline fraction F_c can be estimated by the definition of $F_c = (I_{510} + I_{520})/(I_{480} + I_{510} + I_{520})$, where I_{480}, I_{510} and I_{520} represent integrated intensities of Gaussian peaks near 480, 510 and 520 cm^{-1}, respectively. The obtained data of Raman analysis are also shown in Table 1. Both the slight blue shifts of the crystalline and intermediate peaks, and the reduction of full width

Table 1
The results of Raman and XRD analysis for the silicon films deposited at different substrate temperatures, d_{XRD} is the grain size obtained from XRD.

Substrate temperature (°C)	Crystalline peak position (%)	Intermediate peak position (cm^{-1})	FWHM of the crystalline peak (cm^{-1})	Crystalline fraction (%)	d_{XRD} (nm)
140	–	–	–	0	–
180	517.6	501.2	13.1	46.8	12.8
220	518.0	508.0	9.6	55.8	19.4
260	519.0	510.5	8.3	63.2	23.0
300	519.6	511.8	8.9	66.6	29.2

www.spm.com.cn

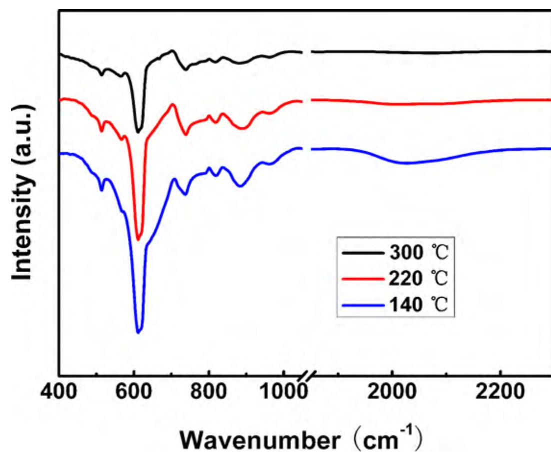

Fig. 3. IR spectra for the silicon films deposited at 140 °C, 220 °C and 300 °C.

at half-maximum (FWHM) of the crystalline peaks results from an increase of crystalline fraction from 0 to 66.6% with increasing the substrate temperature from 140 °C to 300 °C.

The electron density in ICP can reach 10^{11}–10^{12} cm^{-3} in the pressure range of a few to several tens of Pa. The rather high electron density gives rise to a substantial amount of atomic H and SiH_x (x = 1–3) radicals in the plasma. The strong atomic H fluxes can lead to a higher surface coverage to facilitate the migration of SiH_x radicals on the growing surface and the elimination of the broken Si–Si bonds within the subsurface of growing film. The processes are responsible for the effective crystallization of the film deposited at the substrate temperature as low as 180 °C. As the substrate temperature increases, coverage ratio of atomic H on the growing surface and diffusion length of SiH_x radicals increase simultaneously, then the SiH_x radicals can find favorable sites to deposit and form an ordered and well-arranged crystalline structure.

IR spectroscopy was used to investigate the bonding configuration of Si–H and to determine the hydrogen content in the films. Fig. 3 shows IR spectra of the silicon films deposited at 140 °C, 220 °C and 300 °C. The absorption bands at around 620 cm^{-1} are related to the Si–H wagging mode [19] and the bands at 700–900 cm^{-1} are assigned to the stretching/bending modes of Si–H_2 and (Si–H_2)$_n$ complexes [20]. On the other hand, the stretching vibration mode corresponding to monohydride and dihydride bonding can be hardly observed, which usually present between 2000 and 2100 cm^{-1}. These silicon–hydrogen bonding types are generally present in the amorphous silicon matrix and responsible for the degradation of the electrical properties of the amorphous silicon devices [19]. The bonded hydrogen content calculated from

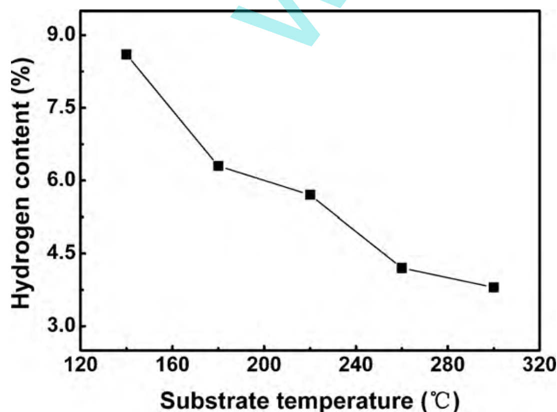

Fig. 4. The calculated hydrogen content as a function of the substrate temperature.

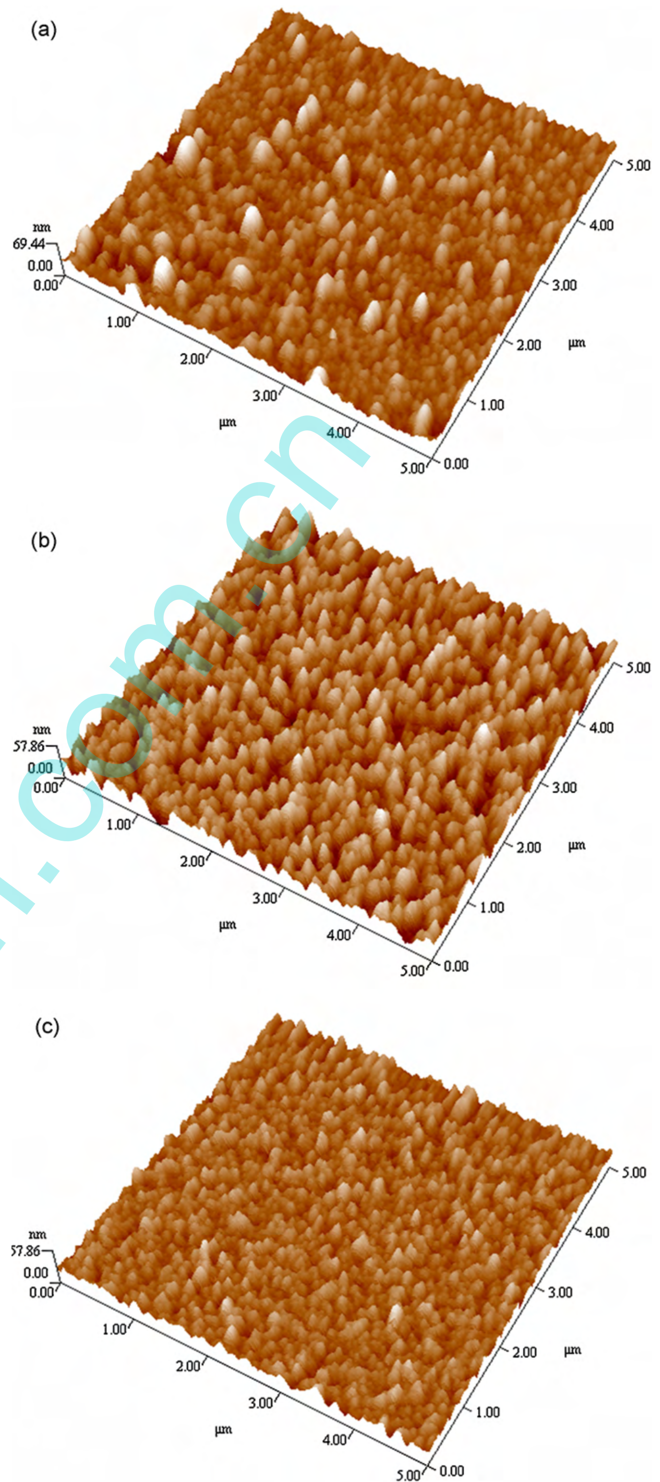

Fig. 5. 3D AFM morphologies of silicon films deposited at (a) 140 °C, (b) 220 °C and (c) 300 °C.

the integrated intensity of the wagging mode is shown in Fig. 4 as a function of the substrate temperature. It can be seen that the hydrogen content gradually decreases with increasing the substrate temperature and reaches a low level of 3.8% at 300 °C. The enhancement of hydrogen desorption from the growing films with increasing the substrate temperature can be responsible for the decrease of hydrogen content. It should be noted that the hydrogen content in all the deposited films is less than 10%.

www.spm.com.cn

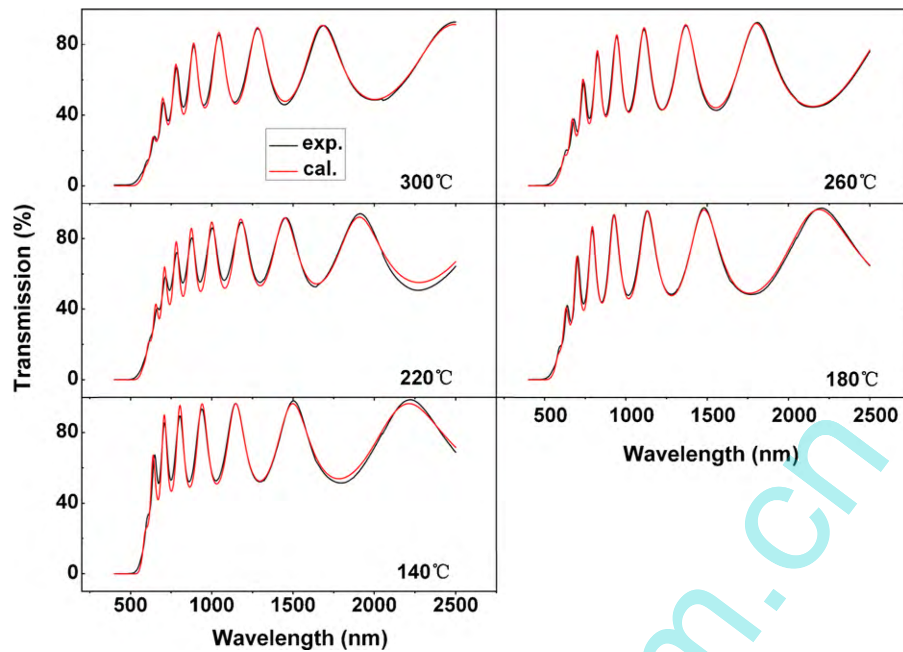

Fig. 6. The experimental and calculated transmission spectra of the silicon films deposited at various substrate temperatures.

The 3D AFM images of the samples prepared at 140 °C, 220 °C and 300 °C are shown in Fig. 5(a)–(c), respectively. For amorphous silicon films deposited at 140 °C, few small heaves can be observed to distribute in the amorphous matrix. When the substrate temperature increases, silicon nanocones in the microcrystalline silicon films present a random and uniform distribution, which is a reflection of the columnar growth. The surface roughness of films decreases as the substrate temperature increases from 220 °C to 300 °C, which is contrary to the reported results [18] where the surface roughness increases with an increase of crystallinity. As shown in Fig. 5, silicon nanocones are more uniformly distributed and the films become more densely packed with increasing the substrate temperature from 220 °C to 300 °C, which leads to a decrease in the surface roughness. The observations agree well with those of the other reports for microcrystalline silicon films [21,22].

3.2. Optical properties

To obtain optical constants of the silicon films from the transmission measurements, we utilized the well-known envelope method to simulate the optical transmission spectra [23–25]. Fig. 6 shows the experimental and calculated transmission spectra of the silicon films deposited at various substrate temperatures. It is obvious that the experimental and calculated data are in excellent agreement with each other. We can retrieve the best-fit values for absorption coefficient and refractive index during the simulation. The optical absorption coefficient spectra of the silicon films deposited at different substrate temperatures are shown in Fig. 7. With an increase of the substrate temperature from 140 °C to 300 °C, the optical absorption coefficient increases, and the film prepared at 300 °C has the maximum optical absorption. In addition, as shown in Fig. 8, the calculated refractive indices at the wavelength of 1.6 μm are found to be enhanced with increasing the substrate temperature. We believe that the densification of the films is responsible for the higher refractive index. In other words, the structure of the films deposited at higher substrate temperatures is less porous and more compact, which has been confirmed by the measurements of AFM as shown in Fig. 5.

Moreover, optical bandgap of silicon films can be calculated from Tauc's formula

$$(\alpha h\nu)^{1/2} = B(h\nu - E_g) \quad (1)$$

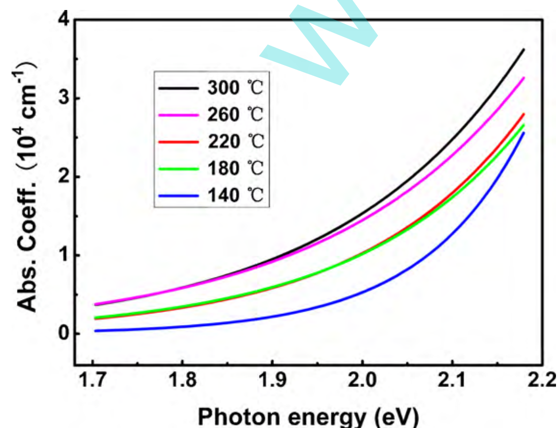

Fig. 7. The optical absorption coefficient spectra of the silicon films deposited at different substrate temperatures.

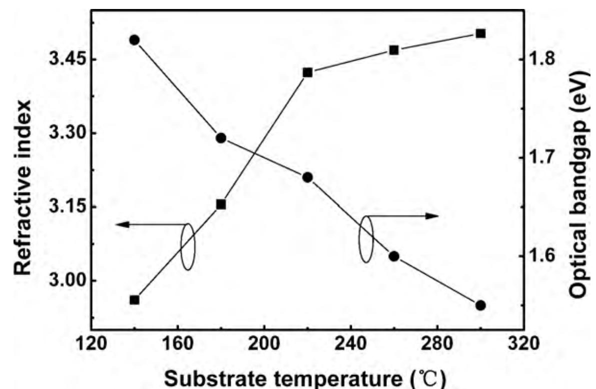

Fig. 8. The refractive index at 1.6 μm and optical bandgap of silicon films as a function of the substrate temperature.

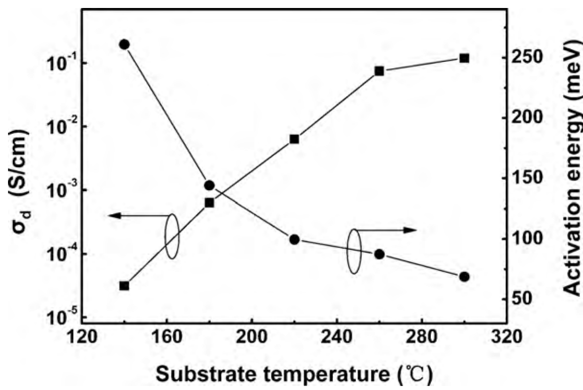

Fig. 9. The dark conductivity at room temperature and activation energy of silicon films deposited at various temperatures.

where α is the absorption coefficient, $h\nu$ is the photon energy, E_g is the energy of the optical bandgap, and B is a constant known as the edge width parameter. From the extrapolation of linear regime in the Tauc plot, the optical bandgap was obtained for the silicon films deposited at different substrate temperatures. As shown in Fig. 8, the optical bandgap narrows with increasing the substrate temperature, and reaches 1.55 eV when the substrate temperature reaches 300 °C. In general, the values of optical bandgap are closely related to the hydrogen content in the films. The higher the hydrogen content, the wider the optical bandgap [26]. As the substrate temperature increases, the narrowing of the optical bandgap shifts the transmission curve towards lower photon energy and enhances the absorption of silicon films in the near-infrared region as shown in Fig. 7. Thus, only by adjusting the substrate temperature, we can tailor the bandgap between 1.5 and 1.8 eV where the photovoltaic conversion efficiency is rather high for single junction solar cell.

3.3. Transport properties

Fig. 9 shows the dark conductivity at room temperature and activation energy of the silicon films deposited at various substrate temperatures. It can be seen that the dark conductivity increases from 3.13×10^{-5} to 1.20×10^{-1} S cm^{-1} accompanied with activation energy decreases from 261.0 to 68.7 meV when the crystallinity of the silicon films increases. We believe that the smaller hydrogen content in our films shown in Fig. 4 leads to a numerous of unsaturated bonds in grain boundary, thus the unsaturated bonds and other structure defects in films can dominate the transport properties of the microcrystalline silicon films. Similar activation energy values can be found in other report [27], where the authors obtained an average activation energy about 40 meV for the microcrystalline silicon films and attributed it to the transitions between defect levels (mean depth about 35 meV inside the energy gap) and the conduction band.

The presence of a high-density of defect levels at grain boundaries affects the density of state distribution at the Fermi level. The variable range hopping (VRH) conductance known to be limited to low-temperature region was observed below 170 K. The dependence of σ on $T^{-1/4}$ for the samples deposited at 180 °C, 220 °C, 260 °C and 300 °C is plotted in Fig. 10. According to Mott law [28] where the carrier transport is dominated by the VRH process, σ may be stated as

$$\sigma = \sigma_{00} \exp\left[-\left(\frac{T}{T_0}\right)^{-1/4}\right] \quad (2)$$

$$T_0 = \frac{16\alpha^3}{kN(E_F)} \quad (3)$$

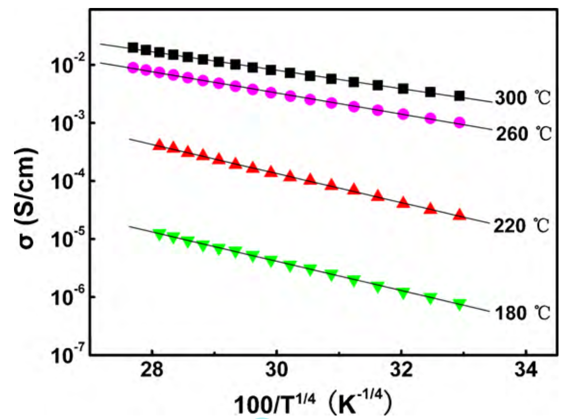

Fig. 10. Dark conductivity σ versus 100 $T^{-1/4}$ for samples deposited at 180 °C, 220 °C, 260 °C and 300 °C.

where σ_{00} is a constant, $1/\alpha$ is the decay length of the wave function of the localized states near the Fermi level, and $N(E_F)$ is the concentration of the localized states at the Fermi level. From Eq. (3) we estimated $N(E_F)$ of the microcrystalline silicon thin films by assuming $1/\alpha$ as 1 nm [29,30]. For samples deposited at 180 °C, 220 °C, 260 °C and 300 °C, the value of $N(E_F)$ are 1.9×10^{19}, 1.7×10^{19}, 5.5×10^{19} and 1.0×10^{20} eV^{-1} cm^{-3}, respectively. These values are consistent with other reports [18,27,29].

4. Conclusions

The microstructure and optoelectronic properties were investigated for the silicon films prepared at different substrate temperatures by ICP-CVD. High-density plasma generated by ICP facilitates the crystallization of silicon films at low temperatures, and microcrystalline silicon films were obtained at a substrate temperature as low as 180 °C. The columnar structure of the films becomes more and more compact with an increase of their crystallinity. The reduction of hydrogen content in the films causes a narrowing of the optical bandgap and an enhancement of the absorption of the silicon films with increasing the substrate temperature. The high dark conductivity and small activation energy in the highly crystalline silicon films were observed near the room temperature, and below 170 K the microcrystalline silicon films show the variable range hopping conductance.

Acknowledgements

This work was supported by the National Natural Science Foundation of China (No. 60776009) and the Natural Science Foundation of Gansu Province (No. 096RJZA056).

References

[1] G. Conibeer, Mater. Today 10 (2007) 42.
[2] L. Tsakalakos, Mater. Sci. Eng. R 62 (2008) 175.
[3] N. Imajyo, J. Non-Cryst. Solids 198–200 (1996) 935.
[4] K. Goshima, H. Toyoda, T. Kojima, M. Nishitani, M. Kitagawa, H. Sugai, Jpn. J. Appl. Phys. 38 (1999) 3655.
[5] N. Kosku, F. Kurisum, M. Takegoshi, H. Takahashi, S. Miyazaki, Thin Solid Films 435 (2003) 39.
[6] C. Niikura, N. Itagaki, M. Kondo, Y. Kawai, A. Matsuda, Thin Solid Films 457 (2004) 84.
[7] H. Shirai, T. Arai, H. Ueyama, Jpn. J. Appl. Phys. 37 (1998) L1078.
[8] H. Jia, J.K. Saha, H. Shirai, Jpn. J. Appl. Phys. 45 (2006) 666.
[9] J. Wang, Y. Qin, H. Yan, P. Gao, J. Li, M. Yin, D. He, Chin. Phys. 18 (2009) 73.
[10] S. Xu, K.N. Ostrikov, Y. Li, E.L. Tsakadze, I.R. Jones, Phys. Plasmas 8 (2001) 2549.
[11] K.N. Ostrikov, S. Xu, M.Y. Yu, J. Appl. Phys. 88 (2000) 2268.
[12] J.H. Lim, K.N. Kim, J.K. Park, J.T. Lim, G.Y. Yeom, Appl. Phys. Lett. 92 (2008) 051504.

www.spm.com.cn

[13] R.A. Stewam, P. Vitello, D.B. Graves, E.F. Jaeger, L.A. Beny, Plasma Sources Sci. Technol. 4 (1995) 36.
[14] Y. Wu, M.A. Lieberman, Plasma Sources Sci. Technol. 9 (2000) 210.
[15] Z. Yu, D. Shaw, P. Gonzales, G.J. Collins, J. Vac. Sci. Technol. A 13 (1995) 871.
[16] K.N. Kim, S.J. Jung, Y.J. Lee, G.Y. Yeom, S.H. Lee, J.K. Lee, J. Appl. Phys. 97 (2005) 063302.
[17] S. Mukhopadhyay, C. Das, S. Ray, J. Phys. D: Appl. Phys. 37 (2004) 1736.
[18] S.Y. Myong, O. Shevaleevskiy, K.S. Lim, S. Miyajima, M. Konagai, J. Appl. Phys. 98 (2005) 054311.
[19] A. Remolina, B.M. Monroy, M.F. García-Sánchez, A. Ponce, M. Bizarro1, J.C. Alonso1, A. Ortiz1, G. Santana, Nanotechnology 20 (2009) 245604.
[20] J.C. Knights, G. Lucovsky, R.J. Nemanich, J. Non-Cryst. Solids 32 (1979) 393.
[21] C. Chen, S. Qiu, C. Liu, Y. Wu, P. Li, C. Yu, X. Lin, J. Phys. D: Appl. Phys. 41 (2008) 195413.
[22] H. Fujiwara, M. Kondo, A. Matsuda, Phys. Rev. B 63 (2001) 115306.
[23] R. Swanepoel, J. Phys. E 16 (1983) 1214.
[24] J. Torres, J.I. Cisneros, G. Gordillo, F. Alvarez, Thin Solid Films 289 (1996) 238.
[25] Z. Tang, W. Wang, B. Zhou, D. Wang, S. Peng, D. He, Appl. Surf. Sci. 255 (2009) 8867.
[26] Q. Cheng, S. Xu, K. Ostrikov, Nanotechnology 20 (2009) 215606.
[27] N. Pinto, M. Ficcadenti, L. Morresi, R. Murri, G. Ambrosone, U. Coscia, J. Appl. Phys. 96 (2004) 7306.
[28] N.F. Mott, Metal–Insulator Transitions, second ed., Taylor & Francis, London, 1990.
[29] F. Liu, M. Zhu, Y. Feng, Y. Han, J. Liu, Thin Solid Films 395 (2001) 97.
[30] S.B. Concari, R.H. Buitrago, M.T. Gutiérrez, J.J. Gandía, J. Appl. Phys. 94 (2003) 2417.

www.spm.com.cn